

Band theory of insulating transition-metal monoxides: Band-structure calculations

K. Terakura and T. Oguchi*

Institute for Solid State Physics, University of Tokyo, Roppongi, Minato-ku, Tokyo 106, Japan

A. R. Williams

IBM Thomas J. Watson Research Center, P.O. Box 218, Yorktown Heights, New York 10598

J. Kübler

Fachgebiet Theoretische Physik, Institut für Festkörperphysik, Hochschulstrasse 2, D-6100 Darmstadt, West Germany

(Received 11 April 1984)

The electronic structure of the insulating antiferromagnetic transition-metal compounds MnO, FeO, CoO, and NiO, which have been regarded as the prototypes of the concept of a Mott insulator, is discussed with use of energy-band theory based on the local-spin-density treatment of exchange and correlation. It is shown that the band structure is very sensitive to the magnetic ordering and that the ground-state magnetic ordering is special in the sense that it makes the e_g (x^2-y^2 , $3z^2-r^2$) band particularly narrow, which is crucial to the insulating nature of NiO. A detailed analysis is made of this particular aspect of the ground-state magnetic ordering. As for FeO and CoO, it is suggested that the population imbalance among the t_{2g} (xy , yz , zx) orbitals induced by the intra-atomic exchange interaction may cause a gap to open at the Fermi level.

I. INTRODUCTION

The transition-metal monoxides MnO, FeO, CoO, and NiO, which are all antiferromagnetic insulators, have occupied a special place in condensed-matter physics for a long-time, because the microscopic origin of their insulating nature¹⁻⁶ and their inter-atomic magnetic coupling is unclear.^{7,8} The common understanding of these problems is that these materials are Mott insulators and that the magnetic coupling is due to super-exchange. Most previous theoretical analyses of the properties of these materials start from the strong correlation limit, i.e., $U/W \gg 1$ with U and W the intra-atomic Coulomb integral and the width of the valence band, respectively.^{2,3,5,6,9} An extensive review on the theories and analysis of experimental data up to 1977 was given by Brandow³ from this point of view. Kunz and co-workers^{4,5} tried to quantify this approach by taking account of correlation effects beyond the Hartree-Fock approximation with the valence-bond approach. The significant results of this calculation are that the unoccupied d states are separated from the occupied ones by about 10 eV and that the gap between the occupied d states and the bottom of the conduction band is 4.8 eV. The large energy separation between the occupied and unoccupied d states is due to the intra-atomic Coulomb interaction and therefore will not be affected by the magnetic ordering. Although some aspects of models characterized by $U/W \gg 1$ are consistent with several experimental results concerning the optical gap and the insulating nature, some of the recent experimental results¹⁰⁻¹³ are not necessarily consistent with the strong-correlation-limit picture. Therefore, it is worthwhile to study the electronic structure of these substances with the self-consistent band-structure theory based on the local-spin-

density-functional method to reexamine the implication of various experimental data.

Wilson¹⁴ was the first to show that MnO and NiO could be band insulators in their ground-state antiferromagnetic ordering, but the result was not sufficiently convincing, because of the lack of the self-consistency in the calculation. An extensive study of the band structures of transition-metal monoxides in the nonmagnetic state was made by Mattheiss.^{15,16} A qualitatively important output of the work was the conjecture that the gap between e_g and t_{2g} subbands would not open up, irrespective of the strength of the p (anion) - d (cation) hybridization in the transition-metal compounds with the NaCl structure. This conjecture was based on the observation that, while the strong p - d hybridization produces a large ligand-field splitting between e_g and t_{2g} subbands, the bandwidth of each subband becomes large at the same time. This conjecture was then one of the causes of Mattheiss's skepticism about the use of band theory for describing the electronic structure of insulating materials MnO, FeO, CoO, and NiO, particularly with reference to the insulating nature above the Néel temperature. An important contribution, which is favorable to band theory, was then made by Andersen *et al.*,¹⁷ who showed that the lattice parameters of the insulating monoxides could be reproduced by the band-structure calculation. In particular, the sudden jump of the lattice parameter from VO to MnO was explained as a magnetic effect. However, their calculation for the ground-state antiferromagnetic orderings was not self-consistent either. (Recent self-consistent calculations by Yamashita and Asano¹⁸ reproduced the observed lattice parameters very well; an almost identical result was obtained by our calculations also.)

In the first two of our series of papers,^{19,20} we presented

some of the results of the self-consistent band-structure calculations for MnO, α -MnS, and NiO in different magnetic states. We showed that the electronic structure is very sensitive to the magnetic ordering and that MnO and NiO can be insulators, but only when the magnetization is allowed to vary in the (111) direction, as it does in the experimentally observed ground state. We call this (111) variation AF II. We then estimated the interatomic magnetic coupling (the exchange interaction parameter in the Heisenberg Hamiltonian) for MnO, α -MnS, and NiO with the use of the muffin-tin coherent-potential-approximation calculation. The theoretical results agree qualitatively with experimental results which were obtained from the spin-wave dispersion curves, thermodynamic analysis, etc.²¹ Our band-theoretical treatment can give natural explanations of the rapid increase of the Néel temperature T_N from MnO ($T_N=122$ K) to NiO ($T_N=523$ K), and also to the small ferromagnetic first-nearest-neighbor coupling in NiO.

In the third paper of this series,²² we demonstrated that a variety of experimental data can be consistently explained with a band picture. In particular, we pointed out that the experimental data of inverse photoemission¹¹ and two-phonon resonant-Raman scattering¹⁰ indicate the presence of d^9 states of Ni in NiO separated from the occupied d band only by ~ 2 eV rather than by ~ 10 eV (a typical value of the Coulomb integral U in the strong-correlation-limit picture). A small (effective) U of about 2 eV for transition-metal monoxides was supported also by Hüffner and Wertheim.²³ Therefore, we take the viewpoint that the effective intra-atomic Coulomb integral U and the energies pertaining to the cation d band are of comparable magnitude. This is in clear contrast to most of the existing Mott-insulator theories for these materials (see, for example, Brandow's review³).

The purpose of the present paper is to give a detailed description of the electronic structure obtained by band theory. In particular, we discuss in detail the reason why the antiferromagnetic ordering AF II is crucial to the insulating state of these oxides. A discussion will also be given on the possibility of having an insulating state for FeO and CoO from a band theory by taking account of the population imbalance in the minority-spin t_{2g} band induced by the intra-atomic exchange interaction. Our important conclusion here is that the difficulty in dealing properly with FeO and CoO lies in the local approximation in the spin-density-functional theory, and not in band theory itself. Analysis of experimental data based on the present band calculations was made in Ref. 22 and will be more extensively made in a subsequent paper.²⁴

The band-structure calculations were done with the augmented-spherical-wave (ASW) method²⁵ and exchange and correlation were treated by the local-spin-density-functional (LSDF) formalism as described in Ref. 26. We use the lattice parameters listed in Table I of Ref. 15.

The organization of the present paper is as follows. We discuss the basic aspects of the band structure of MnO, FeO, CoO, and NiO in Sec. II by presenting several results of the band-structure calculation. In Sec. III we compare our results with some experimental results. We conclude in Sec. IV.

II. RESULTS AND DISCUSSION OF BAND STRUCTURES

A. MnO

1. Overall aspects

Among the four materials (MnO, FeO, CoO, and NiO), MnO is the most easily tractable with regard to the insulating nature in a band picture and yet possesses very informative aspects. Therefore, we begin our discussion with MnO.

Figure 1 shows the total densities of states of MnO in four different magnetic orderings, the ferromagnetic state (F), two antiferromagnetic states, the first kind (AF I) and the second kind (AF II), and the paramagnetic state. (The states below about 0.35 Ry are mostly O $2p$ and those above it are Mn $3d$.) The antiferromagnetic ordering AF I and AF II are schematically shown in Fig. 2. Note that the actual orientation of the magnetic moment with regard to the crystal axis is irrelevant in the present work, because the spin-orbit interaction is not included in our band-structure calculations. A remarkable aspect of

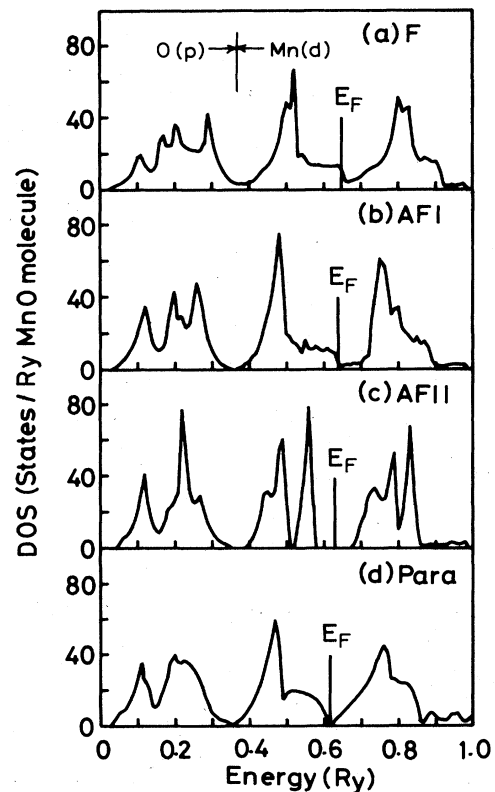


FIG. 1. (a) Total state densities of MnO (in states/Ry/MnO) in the ferromagnetic state, (b) in the antiferromagnetic states of the first kind, AF I, (c) of the second kind, AF II, and (d) in the paramagnetic state. The vertical lines denote the Fermi level.

Fig. 1 is that the ferromagnetic state F and the antiferromagnetic state AF I have similar densities of states and that there is no band gap at the Fermi energy, although the large exchange splitting makes them almost insulators. On the other hand, the antiferromagnetic state AF II, the observed ground-state configuration, has a very narrow e_g band and a well-defined band gap of ~ 0.1 Ry. In the remainder of this section, we focus on the two problems: (i) Why is the e_g band in AF II so narrow compared with that in AF I or F ? (ii) Why is the AF II more stable than AF I or F ?

The schematic energy diagram in Fig. 3 summarizes the formation of d bands in the AF I and AF II structures from atomic levels by including interactions one at a time. We first take account of the exchange splitting Δ_{ex} ($=0.28$ Ry for MnO) and next the ligand-field splitting Δ_{lig} ($=0.08$ Ry for MnO) due to the octahedral cage of oxygen atoms surrounding a cation. Up to this point, there is no difference between AF I and AF II, because no intercation coupling has been taken into account. Important differences between AF I and AF II arise from the next step. First of all, we note that the strongest intercation hopping integral is of the $dd\sigma$ -type between the second-nearest-neighbor cations which is mediated by the oxygen p orbital. The essential difference between AF I and AF II is that this strong $dd\sigma$ interaction couples like polarized cation atoms in AF I, but couples exclusively oppositely magnetized cation atoms in AF II (see Fig. 2). Therefore,

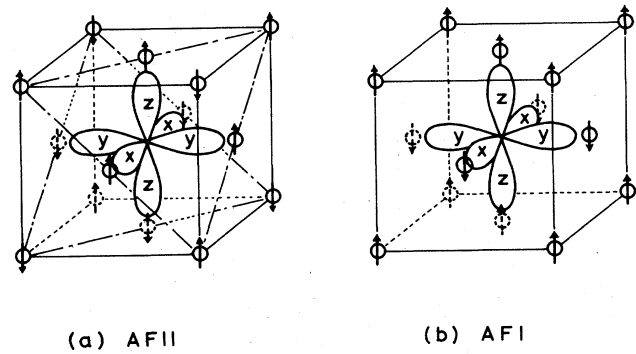


FIG. 2. Antiferromagnetic orderings of the second kind (AF II) and the first kind (AF I). AF II is the ground state ordering for MnO, FeO, CoO, and NiO. (Note that the spin and electronic quantization axes are independent, because of the neglect of the spin-orbit coupling in the present work.) As for the oxygen atoms, only the central one is shown for clarity. In the AF II (AF I) ordering, all three oxygen p orbitals couple action d states belonging to different (same) magnetic sublattices.

inclusion of the intersublattice coupling in AF II causes an appreciable energy shift of e_g states between the majority- and minority-spin bands, while it produces only a negligible effect in AF I. An important consequence of

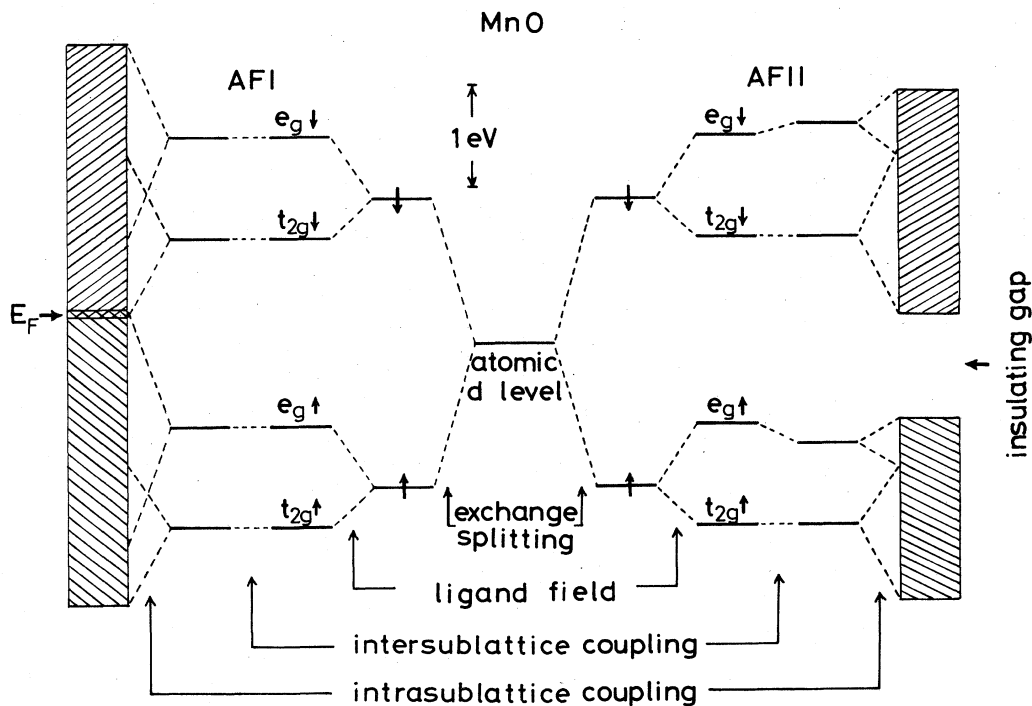


FIG. 3. Schematic diagram showing how the energy bands of d states in AF II and AF I are constructed by including interactions one at a time.

this intersublattice coupling is the stabilization of AF II compared with AF I and also F , due to a larger lowering of the occupied majority-spin e_g states. The final stage, where we take account of the intrasubband banding effect, the e_g subband becomes broader in AF I because of the strong $dd\sigma$ coupling, while the absence of such intrasublattice $dd\sigma$ coupling in AF II leads to a very narrow e_g subband. In addition to the exchange splitting Δ_{ex} , the ligand-field splitting Δ_{lig} is also an important factor for the narrow e_g band in the sense that Δ_{lig} suppresses e_g - t_{2g} hybridization. As for the width of the t_{2g} band, it comes

mostly from the direct first-nearest-neighbor cation-cation coupling and depends on the magnetic ordering only weakly.

The above qualitative arguments will be supplemented by the actual numerical calculations in the next two sections.

2. Intersublattice coupling

Figure 4(a) shows the partial density of states (PDOS) of d states, $n_d(E)$, in AF II of MnO. (See Appendix A for the precise definitions used in the state-density decom-

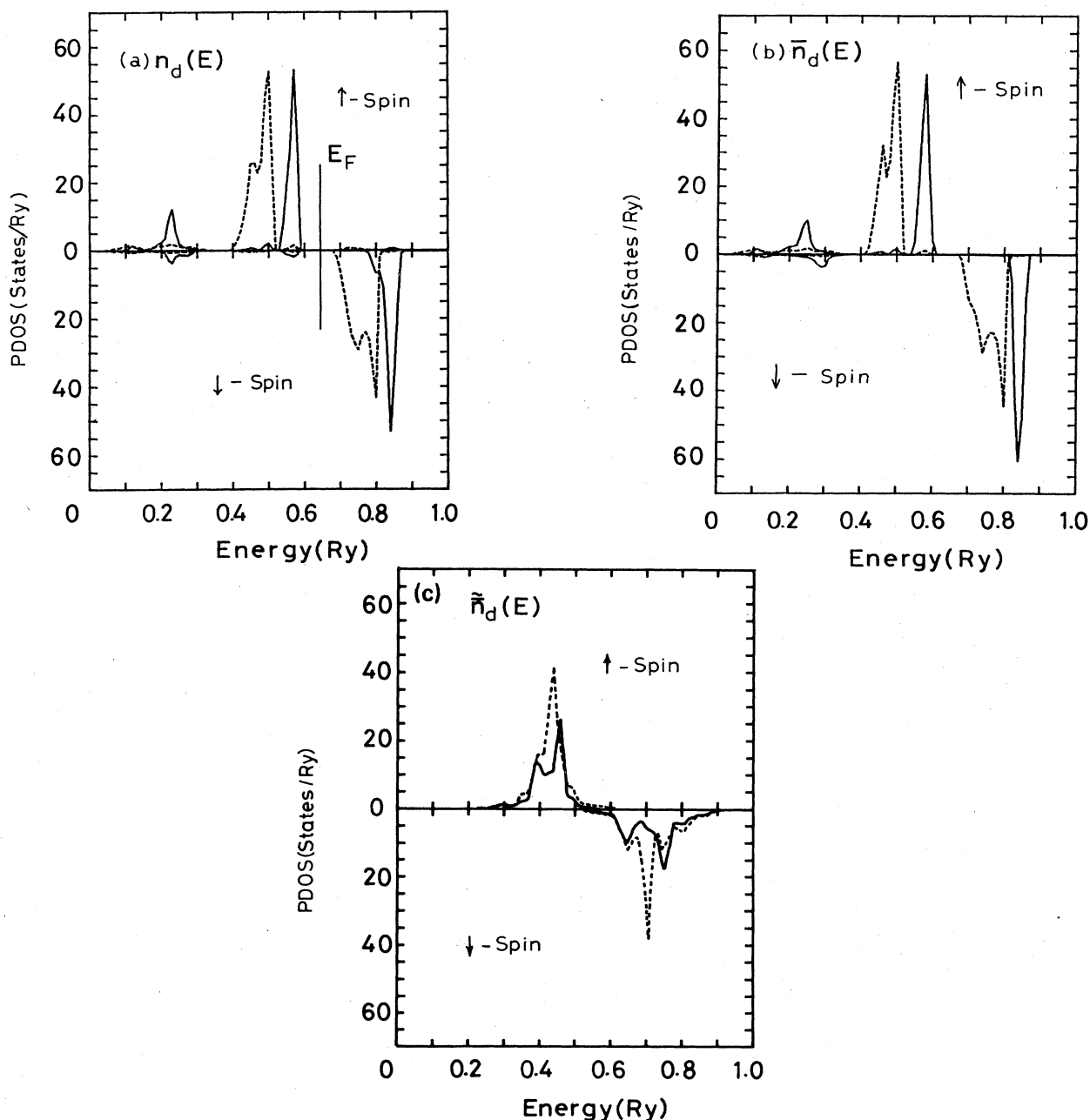


FIG. 4. Partial densities of states for Mn d orbitals in MnO: (a) in the actual AF II ordering, $n_d(E)$; (b) in the absence of the intersublattice hybridization, $\bar{n}_d(E)$; (c) for a spin-up magnetic moment sublattice decoupled from both spin-down magnetic moment sublattice and oxygen sublattice (approximately d PDOS of a single layer of spin-up magnetic moment Mn atoms). The solid (broken) lines denote e_g (t_{2g}) contributions.

position.) The corresponding one without the intersublattice coupling, $\bar{n}_d(E)$, is shown in Fig. 4(b). Note that the strong second-nearest-neighbor $dd\sigma$ coupling is completely absent in the case of Fig. 4(b) and the e_g band is very narrow. (The prescription for removing the intersublattice coupling is given in Appendix B.) At first glance, n_d is almost identical to \bar{n}_d , which implies that the effect of the intersublattice coupling is relatively weak. This is because the large exchange splitting Δ_{ex} suppresses the intersublattice coupling $dd\sigma$ (by a factor of $dd\sigma/\Delta_{ex}=0.08$ in the second-order perturbation theory). The value for $dd\sigma$ was taken from Ref. 15. The weak intersublattice coupling is consistent with the low Néel temperature of MnO ($T_N=122$ K).^{19,20} Nevertheless, by a careful inspection of Figs. 4(a) and 4(b), we notice that there are some differences between n_d and \bar{n}_d and that among these differences, the most significant consequence of the intersublattice coupling is the lowering of the majority-spin e_g band by about 0.02 Ry.

In order to compare the situation in AF II with that in AF I, we show $n_d(E)$ and $\bar{n}_d(E)$ for AF I in Figs. 5(a) and 5(b). As the strong $dd\sigma$ coupling is already included in $\bar{n}_d(E)$, the e_g band is fairly wide and the difference between n_d and \bar{n}_d comes from other weaker couplings. Therefore, any difference in the e_g band between n_d and \bar{n}_d cannot be seen by eye, while small differences in the t_{2g} band exist. The argument in the preceding section about the stabilization of AF II compared with AF I (and F) was thereby substantiated.²⁷ Since the intersublattice hybridization is due to the spin-conserving electron hopping, it is an important concept that the magnetic ordering is determined by the spin-conserving interactions (as opposed to inter-atomic exchange interactions of the Coulomb-interaction origin).

3. Electronic structure of single metal layer

In the preceding section, we calculated the electronic structure of MnO, decoupling the intersublattice hybridization artificially. As a further analysis of the electronic structure, we decouple the oxygen-metal hybridization and calculate the electronic structure of an isolated single magnetic sublattice. (See Appendix B for further details.) From Fig. 2(a), we see that the interlayer distance within a given magnetic sublattice is very large, so that the interlayer interaction within a given sublattice may be negligibly small. Therefore, the PDOS of d states shown in Fig. 4(c) is approximately equal to the one for a single layer of (111) plane of Mn atoms. We note the following features in Fig. 4(c): (1) absence of ligand-field splitting of the d band; (2) a much wider e_g band compared with that of n_d in Figs. 4(a) and 4(b); (3) d density of states in Fig. 4(c) resembles a d resonance in a free-electron sea and the d -band tails from majority- and minority-spin bands overlap to fill the band gap; (4) the width of the d band in Fig. 4(c) is comparable to that of the t_{2g} band in Figs. 4(a) and 4(b); (5) the positions of the d bands are lower than those in Figs. 4(a) and 4(b). The first effect is natural, because there is no O(p)-Mn(d) hybridization. The second results from a large e_g - t_{2g} hybridization caused by the first. The

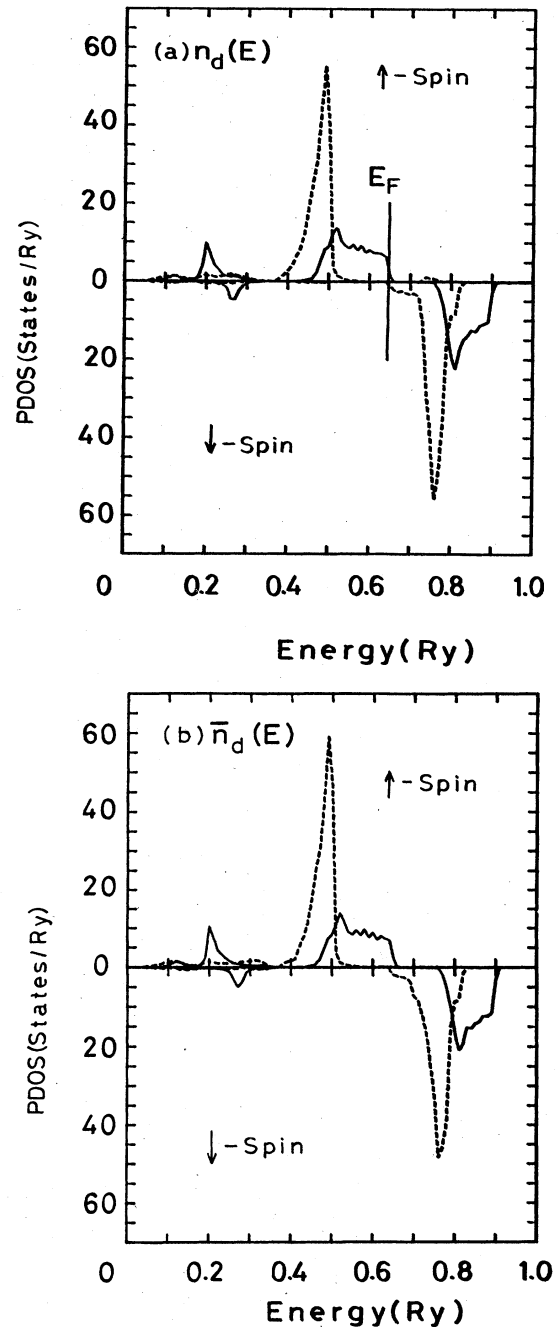


FIG. 5. Partial densities of states for Mn d orbitals: (a) in the actual AF I ordering, $n_d(E)$; (b) in the absence of the intersublattice hybridization, $\bar{n}_d(E)$. The solid (broken) lines denote e_g (t_{2g}) contributions.

third reflects the fact that, in the absence of oxygen, the bottom of the metal s band is lower than the d band, as in the pure transition metal. The fourth indicates that the bandwidth of the t_{2g} band in AF II (and also in AF I) comes mainly from the direct coupling of d orbitals belonging to the neighboring cations. The fifth is due to the absence of repulsion between Mn- d states and O- p states. The first three features are indicative of the important

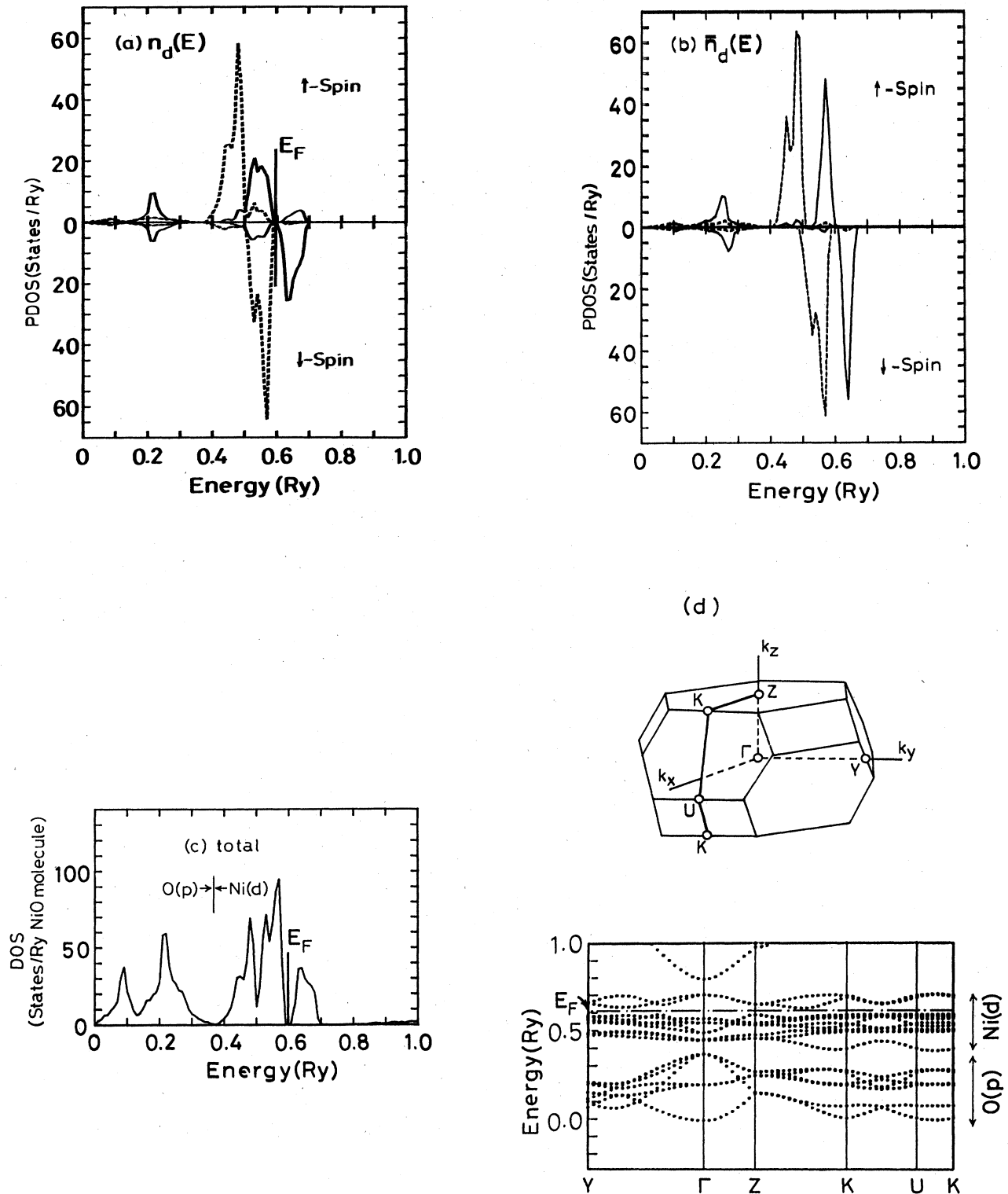


FIG. 6. (a) PDOS of Ni d orbitals in NiO in the actual AF II ordering, $n_d(E)$. (b) PDOS of Ni d orbitals in the absence of the intersublattice hybridization, $\bar{n}_d(E)$. In (a) and (b), the solid (broken) lines denote $e_g(t_{2g})$ contributions. (c) Total density of states per NiO. (d) First Brillouin zone of rhombohedral crystal and the E - \vec{k} curves for the AF II of NiO. The Fermi level E_F is shown by a chain line.

role of oxygen in realizing the insulator state of transition-metal monoxides.

B. NiO

First, the narrow e_g band in AF II is crucial to the insulating nature of NiO, because the Fermi level lies in the e_g-t_{2g} gap in the minority-spin band. It is also crucial to stabilizing the magnetic state. For example, the present band calculation does not produce the magnetic states of *F* and AF I.

Figures 6(a) and 6(b) show PDOS for NiO, $n_d(E)$ and $\bar{n}_d(E)$, which correspond to those of MnO in Fig. 4. The total density of states per NiO and the $E-\vec{k}$ curves are also shown in Figs. 6(c) and 6(d). In contrast to the case of MnO, where the exchange splitting Δ_{ex} dominates the ligand-field splitting Δ_{lig} and width W_d of e_g and t_{2g} subbands, Δ_{ex} in NiO is reduced, because of the smaller atomic magnetic moment, with the result that all of Δ_{ex} , Δ_{lig} , and W_d are comparable in magnitude (~ 1 eV). A reduced Δ_{ex} leads to a much larger intersublattice hybridization. Comparison of the ways of constructing energy bands from atomic levels between MnO and NiO (both in AF II) is schematically shown in Fig. 7. Several interesting aspects can be seen in Figs. 6 and 7. Already in \bar{n}_d , the majority-spin e_g band overlaps the minority-spin t_{2g} band, with the former at a slightly higher energy. The intersubband hybridization between e_g bands pushes the majority-spin e_g band to a lower energy to enhance the overlap between the majority-spin e_g and minority-spin t_{2g} bands, which consequently form a common band. It is

important to note that the fairly large e_g component of the minority spin in the energy range between 0.5–0.6 Ry is not due to the intrasubband e_g-t_{2g} hybridization, but rather to the intersubband e_g-e_g hybridization. The large energy lowering of the majority-spin e_g band by about 0.04 Ry stabilizes the antiferromagnetic ordering AF II and explains the strong antiferromagnetic coupling between the second-nearest-neighbor magnetic moments. In contrast to e_g band, the t_{2g} band is affected only slightly by the hybridization. Because the intersubband $t_{2g}-t_{2g}$ coupling is mainly due to the nearest-neighbor interaction, the small change in the t_{2g} band suggests a weak magnetic coupling between the nearest-neighbor atoms. Although the present analysis cannot predict the sign of the nearest-neighbor coupling, the above results are qualitatively consistent with the experimental results and our previous analysis.^{19,20,28} The larger intersublattice e_g-e_g hybridization due to a smaller exchange splitting in NiO compared with MnO explains also the difference in the Néel temperatures [$T_N=122$ K (MnO), 523 K (NiO)]. This aspect was discussed in our previous papers^{19,20} in terms of the energy denominator in the perturbation treatment of the kinetic superexchange.

C. FeO and CoO

Figures 8(a) and 9(a) show PDOS of *d* states for FeO and CoO in AF II. The Fermi energy lies inevitably within the minority-spin t_{2g} band which has a fairly high density of states and we end up with metallic FeO and CoO. The difficulty cannot be solved even if we take ac-

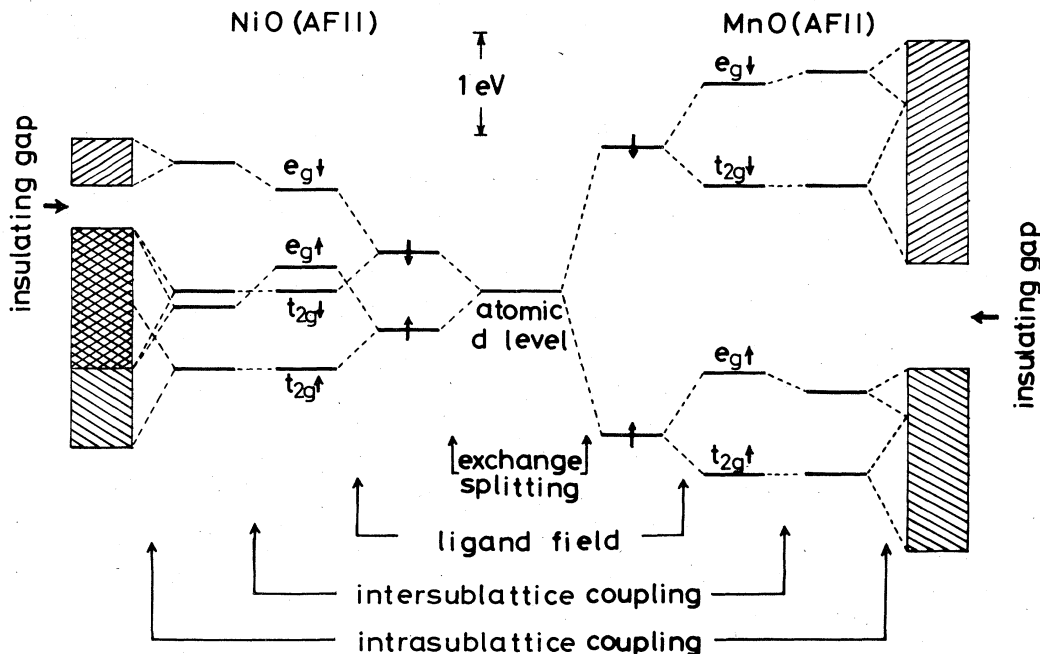


FIG. 7. Schematic diagram showing how the energy bands of *d* states are constructed in NiO and MnO with AF II structure. In the case of MnO, the exchange splitting dominates other energy scales, while in the case of NiO, the exchange splitting, ligand-field splitting and *d*-band width are all comparable in magnitude.

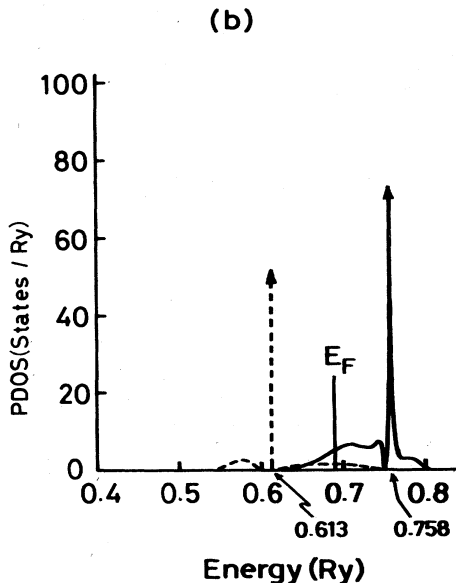
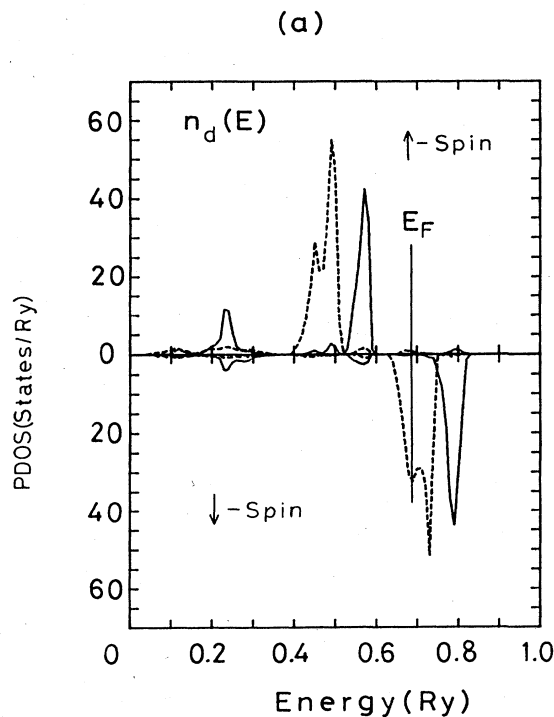


FIG. 8. PDOS of Fe d orbitals in FeO in the AF II ordering without population imbalance in the t_{2g} band of minority-spin state. The solid (broken) lines denote e_g (t_{2g}) contributions. (b) PDOS of Fe t_{2g} orbitals of minority-spin state in FeO with population imbalance only at a given Fe site. The broken curve is a contribution from one of the t_{2g} orbitals which is almost filled and the solid curve is for the other two orbitals. The arrow at 0.613 Ry denotes a split-off state in a gap. There is also a very sharp structure at 0.758 Ry.

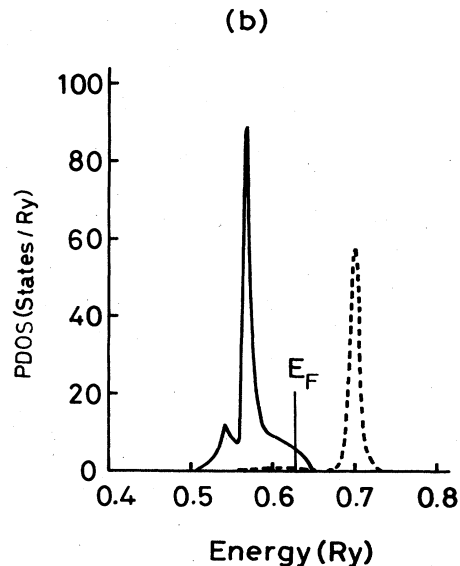
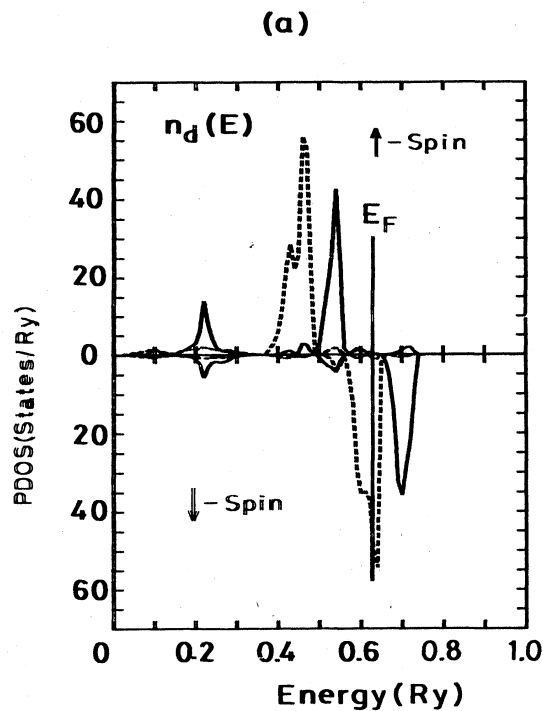


FIG. 9. (a) PDOS of Co d orbitals in CoO in the AF II ordering without population imbalance in the t_{2g} band of minority-spin state. The solid (broken) lines denote e_g (t_{2g}) contributions. (b) PDOS of Co t_{2g} orbitals of minority-spin state in CoO with population imbalance only at a given Co site. The broken curve is a contribution from one of the t_{2g} orbitals which is almost empty and the solid curve is for the other two orbitals.

count of the lattice distortion from the cubic crystal. For instance, CoO has a tetragonal symmetry with $c/a=0.988$ (Ref. 29). First of all, the distortion seems to be too small to produce a gap in t_{2g} band. Besides, even if the ligand field is strong enough to produce a gap, we expect that yz and zx orbitals in the t_{2g} states will have a higher energy than the xy orbital for the distortion of $c/a < 1$. As the t_{2g} band has to accommodate two electrons per metal atom, the Fermi energy must be at the middle of the degenerate yz and zx bands. With these considerations, it has been generally thought that the band theory would never explain the insulating nature of FeO and CoO and that the partial success of the band theory for MnO and NiO would be only accidental.³

We take an opposite viewpoint. We admit that the band theory is not the whole story and that correlation effects beyond the local-density-functional theory will reduce the band width to some extent. However, we found in the previous sections, the insulating nature and the magnetic ordering of MnO and NiO can be explained in a quite natural way within the band picture. This encourages us to think that the band theory should at least indicate an inclination of FeO and CoO to becoming an insulator. The key which has been missing is the presence of a fairly large unquenched orbital angular momentum in both materials. An extensive study of the orbital angular momentum in CoO was made by Kanamori.³⁰ The fundamental implication of a significant orbital moment in the present context is the instability to the population imbalance in the minority-spin t_{2g} band induced by the intra-atomic exchange interaction. By using the Anderson model or the tight-binding model with degenerate orbitals, it was shown that the condition of the population imbalance is given by³¹⁻³³

$$n(E_F)(U-J) > 1, \quad (1)$$

where $n(E_F)$ is the density of states per spin and per orbital at the Fermi level. U and J are the Coulomb and exchange integrals. Yosida *et al.*³² analyzed the anisotropy energy of transition-metal impurities in Co metal and estimated the values of $U-J$ as 2 eV, with U and J as 3 and 1 eV, respectively, for the $3d$ transition elements. With the use of $n(E_F)$ obtained by the present band calculations, we obtain

$$n(E_F)(U-J) = \begin{cases} 2.5, & \text{for CoO,} \\ 1.8, & \text{for FeO.} \end{cases} \quad (2)$$

Therefore, we expect that FeO and CoO are unstable with regard to the population imbalance in the t_{2g} band, which indicates the possibility of opening up a gap at the Fermi level.

One of the ways of checking the reliability of the above values of U and J is to study the Stoner criterion for the instability to the formation of the spin-magnetic moment, for which analyses based on the local-spin-density-functional formalism are also available.^{34,35} The condition is given by

$$n(E_F)(U+4J) > 1, \quad (4)$$

where the factor of 4 before J is obtained for the d -band case. First we note that the exchange integral I by Janak³⁴ corresponds to $(U+4J)/10$, because Janak used the density of states which includes both the spin and the orbital degeneracies. The estimate by Yosida *et al.* of U and J gives $(U+4J)/10=0.052$ Ry, which is about 1.4 times larger than Janak's I of 0.036 Ry. The use of the above values for U and J is, however, rather reasonable for FeO and CoO, because it is generally expected that U and J will take larger values in compounds (than in pure metals), due to the absence of the screening effects of s electrons. We note also that even if we reduce $U-J$ by 1.4, the condition of Eq. (1) is still satisfied for FeO and CoO.³⁶

Deferring a more extensive study to future work, we present here some results obtained by a simple model calculation in order to demonstrate the significance of the population imbalance for making FeO and CoO insulators. What we do is as follows. We take account of the possibility of the population imbalance only at a given Co (or Fe) site, leaving other sites as shown in Figs. 8(a) and 9(a). Therefore the problem is reduced to an impurity problem and we solve it approximately by using linear combination of atomic orbitals (LCAO) formalism, which will work for the narrow t_{2g} band of present interest. The inputs to the calculation are the PDOS of t_{2g} [Figs. 8(a) or 9(a)] and the value of $U-J$. By setting $U-J=2$ eV, a self-consistent solution with the population imbalance in the minority-spin t_{2g} band is shown in Figs. 8(b) and 9(b) for FeO and CoO, respectively. Because this is an impurity problem, the density of states at the central site (impurity site) cannot have a gap at the Fermi level. Nevertheless, it is clear that the PDOS of t_{2g} in Figs. 8(b) and 9(b) consists of two almost separate bands with very small values of state densities at the Fermi level. If the population imbalance occurs at every site, each of the sharp separate states will become broader but the tails will shrink and thereby a gap will open up at the Fermi level.

One may think that we should do the above analysis within the framework of the local-spin-density-functional formalism. Unfortunately, the LSDF formalism is not adequate for the estimation of the energy change caused by the symmetry breaking in the charge distribution.³⁷ Actually our estimation by the LSDF of the quantity corresponding to $U-J$ turned out to be negative, which is apparently unphysical (see Appendix C). We have to go beyond the LSDF formalism in order to deal with the unquenched orbital angular momentum properly. We are claiming that the present difficulty in dealing with FeO and CoO lies in the local approximation of the density-functional theory, but not in the band theory itself.

III. COMPARISON WITH SOME EXPERIMENTAL DATA

Since extensive analyses of experimental data are made in other papers,^{22,24} here we only present calculated results for the magnitude of the local magnetic moment of cation and also for the ligand-field splitting.

A. Magnitude of the cation magnetic moment

Experimentally, the magnitude of the magnetic moment associated with a cation is obtained by the analysis of the magnetic form factor. The experimental values (in μ_B) are 4.79 for MnO (Ref. 38), 1.64 (Ref. 39) and 1.77 (Ref. 38) for NiO, and 3.35 (Ref. 40) for CoO. [In the case of NiO, the spin-magnetic moment was obtained by taking account of the g factor of 2.2 (Ref. 39) and the value for CoO includes a contribution from the orbital angular momentum.] The experimental value for FeO is not available to our knowledge.

In our band-structure calculation, the magnetic moment of a metal atom, M_{loc} , is defined as the spin magnetic moment within the atomic sphere of metal atom. Naively, one may think that M_{loc} would simply be 5 and 2 for MnO and NiO, respectively, because a gap exists at the Fermi level. This is not true. First, the intersubband hybridization introduces a mixing between the local majority- and minority-spin states. Therefore, in the occupied Mn d bands, there is a small contribution from the local minority-spin states, which reduces the value of M_{loc} . In addition, there is also a contribution from the hybridization with the oxygen p states, which do not have spin polarization. In this way, M_{loc} for Mn is reduced to 4.45. Similarly, M_{loc} for other materials are 3.43 (FeO), 2.35 (CoO), and 1.09 (NiO). We see that the experimental values listed above are larger than the theoretical M_{loc} , particularly for NiO. (We leave the discussion of FeO and CoO to a future work.) It is important to note here that M_{loc} depends on the choice of atomic radius of each species, and does not exactly correspond to the experimental values. Figure 10 shows the dependence of M_{loc} on the ratio of atomic radii R_{Ni}/R_O for NiO with a fixed lattice constant. The amount of charge transfer Q from an atomic sphere of Ni to that of O is also shown. Our usual prescription for determining atomic radius for each element in a compound⁴¹ gives 1.13 as R_{Ni}/R_O and Pauling's ionic radii for Ni^{2+} and O^{2-} give about 0.5.⁴² The rather sensitive dependence of M_{loc} on the choice of atomic radii comes from the spatial spin polarization around oxygen atoms, although they do not have net spin polarization. When we change the radius of the atomic sphere of oxygen, the spatial spin polarization around oxygen makes a contribution to M_{loc} of metal atom effectively. This implies deviations from the spherical-potential approximation used in the present band calculation. It is one of our future projects to calculate the spin-density distribution or the magnetic form factor with the

TABLE I. Theoretical and experimental ligand-field splitting in the ground state (in Ry).

	MnO	FeO	CoO	NiO
Theory	0.077	0.084	0.085	0.099
Experiments ^a	0.089		0.086	0.083
	0.092			0.081
				0.080

^aExperimental data are borrowed from Table I in Ref. 16.

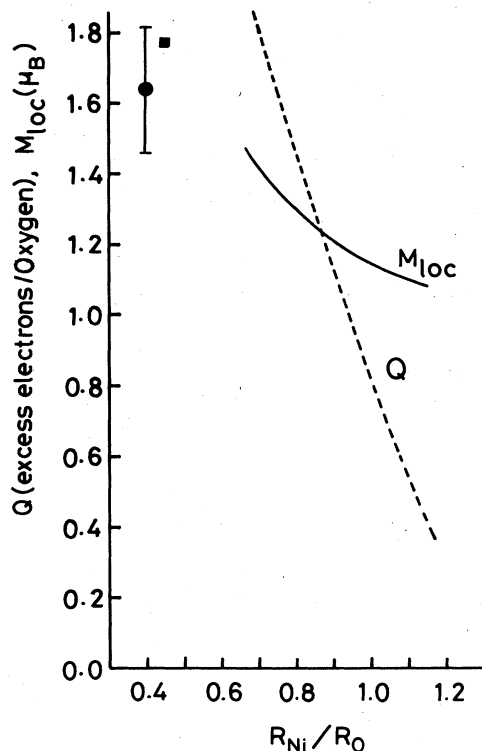


FIG. 10. Spin magnetic moment within the atomic sphere of Ni in NiO, M_{loc} (in μ_B), and the electron transfer from Ni to O, Q , are shown as functions of R_{Ni}/R_O . The experimental data for Ni magnetic moment are shown also by a square (Ref. 38) and a circle with an error bar (Ref. 39).

use of a more general form of the potentials in the band calculation and thereby to make a direct comparison with theory and experiment.

B. Ligand-field splitting

Table I shows the ligand-field-splitting data. Theoretical values were obtained by calculating the difference in the energy of the centers of gravity of t_{2g} and e_g bands. The agreement between theory and experiment is satisfactory. It should be noted that the t_{2g} - e_g splitting is entirely due to the p - d covalency effect in the present calculation, because of the use of the spherical potential for metal atoms. Because the charge associated with oxygen spreads widely in space, the electrostatic contribution to the ligand-field splitting must be very small. In contrast to our results, Mattheiss¹⁶ underestimated the ligand-field splitting. The main source of this discrepancy is his underestimation of the p - d covalency effect due to a much larger energy separation between oxygen p band and metal d band in his band scheme.

IV. CONCLUSIONS

We have shown that the band theory based on the LSDF formalism accounts well for the insulating nature of MnO and NiO in their ground-state magnetic ordering

AF II. The antiferromagnetic ordering AF II is special in the sense that it makes the e_g band particularly narrow. This is a crucial condition for making MnO and NiO insulators. The reasons for the narrow e_g band in AF II and the stability of AF II were analyzed in detail. As for the insulating nature of FeO and CoO, we pointed out the possibility of having a population imbalance among the t_{2g} states, which is induced by the intra-atomic exchange interaction and is related to the unquenched orbital angular momentum in these materials. We showed that the partial density of states from the present band calculation satisfies the criterion for the instability for the population imbalance for the values of the Coulomb and exchange integrals, U and J , estimated from the anisotropy energy of transition-metal impurities in metallic cobalt.³² (Note that we assumed that $U - J$ is 2 eV rather than about 10 eV, the latter being the commonly used value in strong correlation-limit picture.^{3,36}) We then demonstrated by a model calculation that the population imbalance splits the minority-spin t_{2g} band into two almost separate subbands with only a very small density of states at the Fermi level. However, the LSDF formalism leads us to a rather unphysical result in this problem (Appendix C).³⁷

We showed that the ligand-field splitting calculated by our band calculations agrees fairly well with observed one. An important concept here is that the covalency effect between oxygen p states and metal d states is the dominant source of the ligand-field splitting. Calculated local magnetic moment is generally smaller than that observed by neutron diffraction. However, it was pointed out that some fundamental difficulties exist in making a direct comparison of the cation magnetic moment between theory and experiment.

In a subsequent paper, we will give an extensive analysis of experimental data from our band scheme, discuss some possible mechanisms to sustain the insulating nature even above the Néel temperature and show that the oxides MnO, FeO, CoO, and NiO are much less special than is generally thought.

Note added in proof. After submission of the manuscript, S. Wakoh informed us of his work about the population imbalance in CoO [S. Wakoh, J. Phys. F 7, L15 (1977)].

ACKNOWLEDGMENTS

The authors would like to thank N. Hamada for valuable comments and discussions. They are also grateful to V. Moruzzi for invaluable help with the numerical computations. This work was initiated while one of the authors (K.T.) was visiting at the IBM Thomas J. Watson Research Center (Yorktown Heights). He would like to express his sincere thanks to the IBM World Trade Corporation for supporting his stay here. This work was supported in part by a Grant-in-Aid for Cooperative Research from the Ministry of Education, Science and Culture of Japan.

APPENDIX A: PARTIAL-DENSITY-OF-STATES (PDOS) DECOMPOSITION IN AF II

In the PDOS shown in Figs. 4, 5, 6, 8, and 9, e_g and t_{2g} states are referred to with regard to the cubic axes of the

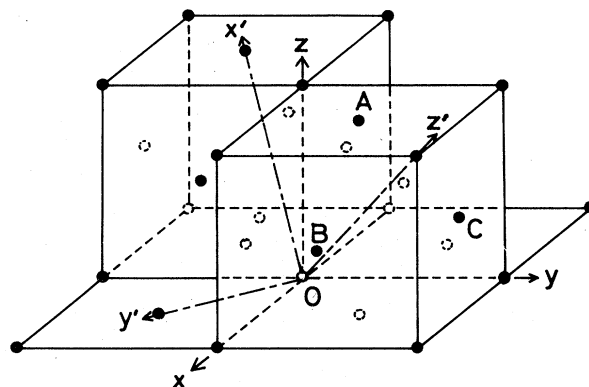


FIG. 11. Relation of two coordinate systems. The x , y , and z axes are along the cubic crystal axes. The x' , y' , and z' axes are taken so that the z' axis is the threefold rotation axis, the z' - x' plane is the mirror plane, and the y' axis is the twofold rotation axis in the case of the AF II ordering. Only the cations are shown by circles.

NaCl structure. As the point-group symmetry of the AF II is D_{3d} , the orbitals belonging to e_g and t_{2g} are not the basis functions of the irreducible representations of D_{3d} . By taking the new x' , y' , and z' axes, as shown in Fig. 11 [(z' , x') plane is the mirror plane and y' axis is the twofold rotation axis], the five d orbitals are categorized into three groups according to the irreducible representations of D_{3d} : $|3(z')^2 - r^2\rangle$, A_1 ; $|y'z'\rangle$ and $|z'x'\rangle$, $E(1)$; $|x'y'\rangle$ and $-(x')^2 - (y')^2$, $E(2)$.

The argument of E identifies two different sets of basis functions belonging to the irreducible representation E . The above d orbitals are expressed by e_g and t_{2g} orbitals as

$$\begin{aligned} |3(z')^2 - r^2\rangle &= (|xy\rangle + |yz\rangle + |zx\rangle)/\sqrt{3}, \\ |y'z'\rangle &= (2|x^2 - y^2\rangle - |yz\rangle + |zx\rangle)/\sqrt{6}, \\ |z'x'\rangle &= \sqrt{2/3} |3z^2 - r^2\rangle \\ &\quad - (\sqrt{2}/6)(2|xy\rangle - |yz\rangle - |zx\rangle), \\ |x'y'\rangle &= -(|x^2 - y^2\rangle + |yz\rangle - |zx\rangle)/\sqrt{3}, \\ |(x')^2 - (y')^2\rangle &= (1/\sqrt{3}) |3z^2 - r^2\rangle \\ &\quad + (1/3)(2|xy\rangle - |yz\rangle - |zx\rangle). \end{aligned}$$

We take linear combinations between $E(1)$ and $E(2)$ to obtain the following new set of functions:

$$\begin{aligned} \phi_1 &= (1/\sqrt{3})(|xy\rangle + |yz\rangle + |zx\rangle) \\ &= |3(z')^2 - r^2\rangle, \\ \phi_2 &= (1/\sqrt{2})(|zx\rangle - |yz\rangle) \\ &= (1/\sqrt{3})(|y'z'\rangle + \sqrt{2}|x'y'\rangle), \\ \phi_3 &= (1/\sqrt{6})(-2|xy\rangle + |yz\rangle + |zx\rangle) \\ &= (1/\sqrt{3})[|z'x'\rangle - \sqrt{2}|(x')^2 - (y')^2\rangle], \end{aligned}$$

$$\begin{aligned}\phi_4 &= |x^2 - y^2\rangle = (1/\sqrt{3})(\sqrt{2}|y'z'\rangle - |x'y'\rangle), \\ \phi_5 &= |3z^2 - r^2\rangle \\ &= (1/\sqrt{3})[\sqrt{2}|z'x'\rangle + |(x')^2 - (y')^2\rangle].\end{aligned}$$

The PDOS of t_{2g} and e_g are defined as

$$\begin{aligned}n_{t_{2g}} &= -(1/\pi)\text{Im}(\langle xy | G | xy \rangle + \langle yz | G | yz \rangle \\ &\quad + \langle zx | G | zx \rangle), \\ n_{e_g} &= -(1/\pi)\text{Im}(\langle x^2 - y^2 | G | x^2 - y^2 \rangle \\ &\quad + \langle 3z^2 - r^2 | G | 3z^2 - r^2 \rangle),\end{aligned}$$

where G is the Green function of the system. It is now straightforward to show that

$$\begin{aligned}n_{t_{2g}} &= -(1/\pi)\text{Im}(\langle \phi_1 | G | \phi_1 \rangle \\ &\quad + \langle \phi_2 | G | \phi_2 \rangle + \langle \phi_3 | G | \phi_3 \rangle) \\ &= n_{A_1} + \frac{1}{3}(n_{E(1)} + 2n_{E(2)} + 2\sqrt{2}n_{E(1-2)}), \\ n_{e_g} &= -(1/\pi)\text{Im}(\langle \phi_4 | G | \phi_4 \rangle + \langle \phi_5 | G | \phi_5 \rangle) \\ &= \frac{1}{3}(2n_{E(1)} + n_{E(2)} - 2\sqrt{2}n_{E(1-2)}),\end{aligned}$$

where

$$\begin{aligned}n_{A_1} &= (1/\pi)\text{Im}(\langle 3(z')^2 - r^2 | G | 3(z')^2 - r^2 \rangle), \\ n_{E(1)} &= -(1/\pi)\text{Im}(\langle y'z' | G | y'z' \rangle \\ &\quad + \langle z'x' | G | z'x' \rangle), \\ n_{E(2)} &= -(1/\pi)\text{Im}[\langle x'y' | G | x'y' \rangle \\ &\quad + \langle (x')^2 - (y')^2 | G | (x')^2 - (y')^2 \rangle], \\ n_{E(1-2)} &= -(1/\pi)\text{Im}[\langle y'z' | G | x'y' \rangle \\ &\quad - \langle z'x' | G | (x')^2 - (y')^2 \rangle].\end{aligned}$$

n_{A_1} , $n_{E(1)}$, $n_{E(2)}$, and $n_{E(1-2)}$ can be obtained by the k -space integration in the irreducible part of the Brillouin zone. The off-diagonal part $n_{E(1-2)}$ makes a significant contribution.

In the actual density-of-states (DOS) or PDOS calculations for the AF II structure, 810 \bar{k} points, which are equally spaced in the irreducible part of the Brillouin zone, are used and the spectral weight corresponding to each eigenstate is broadened by an isosceles triangle with the base width of 0.01 Ry. (Therefore, in the DOS curves, a gap is smaller than the real value. However, the value of a gap referred to in the text is obtained by sampling the highest occupied eigenenergy and the lowest unoccupied one and is not affected by the broadening effect.) For the AF I structure, 550 \bar{k} points are used.

APPENDIX B: COMMENTS ON $n_d(E)$ AND $\bar{n}_d(E)$ IN FIGS. 4–6

The secular equation in augmented spherical waves²⁵ (ASW) can be formally written as

$$\det \begin{bmatrix} A_{M1,M1} & A_{M1,M2} & A_{M1,O} \\ A_{M2,M1} & A_{M2,M2} & A_{M2,O} \\ A_{O,M1} & A_{O,M2} & A_{O,O} \end{bmatrix} = 0, \quad (\text{B1})$$

where the subscript $M1$ ($M2$) denotes the metal sublattice of \uparrow (\downarrow) magnetic moment in Fig. 2 and the subscript O the oxygen sublattice. By using the matrix transformation of Eq. (27) of Ref. 43, we can fold the oxygen subspace into the metal subspace and reduce (B1) into

$$\det \begin{bmatrix} B_{M1,M1} & B_{M1,M2} \\ B_{M2,M1} & B_{M2,M2} \end{bmatrix} = 0, \quad (\text{B2})$$

with

$$B_{Mi,Mj} = A_{Mi,Mj} - A_{Mi,O}(A_{O,O})^{-1}A_{O,Mj}. \quad (\text{B3})$$

The off-diagonal blocks $B_{M1,M2}$ and $B_{M2,M1}$ contribute to the intersublattice hybridization. $n_d(E)$ in Figs. 4–6, are obtained from either (B1) or (B2) and its counterpart $\bar{n}_d(E)$ from either

$$\det(B_{M1,M1}) = 0, \quad (\text{B4})$$

or

$$\det \begin{bmatrix} A_{M1,M1} & A_{M1,O} \\ A_{O,M1} & A_{O,O} \end{bmatrix} = 0. \quad (\text{B5})$$

Furthermore, the d PDOS of Fig. 4(c) is calculated simply by

$$\det(A_{M1,M1}) = 0. \quad (\text{B6})$$

An additional comment on (B5) and (B6) is that the matrix elements in (B5) and (B6) are not exactly the same as the corresponding ones in (B1). In the ASW formalism,²⁵ the $M2$ sublattice makes some contribution to, for example, $A_{M1,M1}$. [This comes from the sum over ν'' in Eq. (29) of Ref. 25.] Such a contribution is included in (B1), but is artificially neglected in (B5). In (B6), contributions from both of $M2$ and oxygen sublattices to $A_{M1,M1}$ are neglected.

APPENDIX C: A NOTE ON THE LSDF APPROACH TO THE ARGUMENT IN SEC. II C

Let us assume the charge-density fluctuation at a Co site represented by

$$\begin{aligned}\delta\rho(\vec{r}) &= \delta n \{ -[Y_{yz}(\vec{r})]^2 + 0.5[Y_{xy}(\vec{r})]^2 \\ &\quad + 0.5[Y_{zx}(\vec{r})]^2 \} [R_d(r; E_F)]^2, \quad (\text{C1})\end{aligned}$$

where $Y_L(\vec{r})$ denotes the real spherical harmonics and $R_d(r; E_F)$ is the radial wave function of Co with the Fermi energy which is normalized to unity within the atomic sphere. $\delta\rho(\vec{r})$ of (C1) represents the situation where a fractional charge δn is transferred from the yz state to the xy and zx states. If CoO is unstable with respect to this charge fluctuation, a situation where the yz state will have a higher energy than the xy and zx states will be spontaneously realized and there is a possibility of having a gap which separates the unoccupied yz state from the occupied xy and zx states. $\delta\rho$ of (C1) will give the energy shift $\delta\epsilon$ for the yz orbital given as

$$\delta\epsilon = \left\langle yz \left| \left[\frac{\partial U_{xc}}{\partial \rho} \delta\rho(\vec{r}) + 2 \int \frac{\delta\rho(\vec{r}')}{|\vec{r}-\vec{r}'|} d^3r' \right] \right| yz \right\rangle. \quad (C2)$$

The criterion for the charge imbalance is given by

$$n_{yz}(E_F)\delta\epsilon > \delta n, \quad (C3)$$

where n_{yz} is the PDOS for the yz orbital. We can reduce (C3) to

$$n_{yz}(E_F) \{ \{ \delta\epsilon(\text{Coul})_{\text{off-dia}} - [\delta\epsilon(\text{Coul})]_{\text{dia}} \} + \{ [\delta\epsilon(\text{XC})]_{\text{off-dia}} - [\delta\epsilon(\text{XC})]_{\text{dia}} \} \} > 1, \quad (C4)$$

which corresponds to Eq. (1). In (C4), the subscript dia denotes the contribution to $\delta\epsilon$ of (C2) from the charge fluctuation associated with the yz orbital and the subscript off-dia denotes the contribution from the xy or zx orbital. The quantities in (C4) are expressed as

$$[\delta\epsilon(\text{Coul})]_i = \sum_{l=0,2,4} \alpha_{l,i} \lambda_l, \quad i = \text{off-dia or dia},$$

with

$$\lambda_l = 2 \int_0^R dr [R_d(r; E_F)]^2 \times \left[r^{l-1} \int_0^r [R_d(r'; E_F)]^2 (r')^{l+2} dr' + r^{l+2} \int_r^R [R_d(r'; E_F)]^2 (r')^{l-1} dr' \right],$$

$$\alpha_{l,\text{dia}} = \begin{cases} 1, & l=0, \\ \frac{4}{49}, & l=2,4, \end{cases}$$

$$\alpha_{l,\text{off-dia}} = \begin{cases} 1, & l=0, \\ -\frac{2}{49}, & l=2, \\ -\frac{4}{441}, & l=4, \end{cases}$$

and

$$[\delta\epsilon(\text{XC})]_{\text{dia}} = \left(\frac{15}{28} \pi \right) \eta,$$

$$[\delta\epsilon(\text{XC})]_{\text{off-dia}} = \left(\frac{5}{28} \pi \right) \eta,$$

with

$$\eta = \int_0^R \frac{\partial U_{xc}}{\partial \rho} [R_d(r; E_F)]^4 r^2 dr.$$

With the use of the self-consistent potential for Co, we estimated λ_l and η as (in Ry)

$$\lambda_l = \begin{cases} 1.8360, & l=0 \\ 0.8385, & l=2 \\ 0.5195, & l=4 \end{cases}$$

and

$$\eta = -1.0184.$$

With these values we obtain

$$[\delta\epsilon(\text{Coul})]_{\text{dia}} = 1.9468,$$

$$[\delta\epsilon(\text{Coul})]_{\text{off-dia}} = 1.7970,$$

$$[\delta\epsilon(\text{XC})]_{\text{dia}} = -0.1737,$$

$$[\delta\epsilon(\text{XC})]_{\text{off-dia}} = -0.0579,$$

in Ry and the value in the bold parentheses on the left-hand-side of (C4) is -0.034 Ry. This value corresponds to $U-J$ in Eq. (1) and the negative value is unphysical. One of the shortcomings of the present scheme compared with that in Sec. II C, which is based on the Hartree-Fock scheme, is due to the nonvanishing contribution of the self-energy.

*Present address: Department of Physics and Astronomy, Northwestern University, Evanston, IL 60201.

¹N. F. Mott, Proc. Phys. Soc. London Ser. A **62**, 416 (1949).

²D. Adler, *Solid State Physics*, edited by F. Seitz and D. Turnbull (Academic, New York, 1968), Vol. 21, p. 1.

³B. H. Brandow, Adv. Phys. **26**, 651 (1977).

⁴A. B. Kunz and G. T. Surratt, Solid State Commun. **25**, 2989 (1978).

⁵A. B. Kunz, Int. J. Quantum Chem. Symp. **15**, 487 (1981).

⁶B. Koiller and L. M. Falicov, J. Phys. C **7**, 299 (1974).

⁷P. W. Anderson, in *Solid State Physics*, edited by F. Seitz and D. Turnbull (Academic, New York, 1963), Vol. 14, p. 99.

⁸B. Koiller and L. M. Falicov, J. Phys. C **8**, 695 (1975).

⁹D. Adler and J. Feinleib, Phys. Rev. B **2**, 3112 (1970).

¹⁰R. Merlin, T. P. Martin, A. Polian, M. Cardona, B. Andlauer, and D. Tannhauser, J. Magn. Magn. Mater. **9**, 83 (1978).

¹¹H. Scheidt, M. Glöbl, and V. Dose, Surf. Sci. **112**, 97 (1981).

¹²S. J. Oh, J. W. Allen, I. Lindau, and J. C. Mikkelsen, Jr., Phys. Rev. B **26**, 4845 (1982).

¹³M. R. Thuler, R. L. Benbow, and Z. Hurych, Phys. Rev. B **27**,

2082 (1983).

¹⁴T. M. Wilson, Int. J. Quantum Chem. Symp. **3**, 757 (1970).

¹⁵L. F. Mattheiss, Phys. Rev. B **5**, 290 (1972).

¹⁶L. F. Mattheiss, Phys. Rev. B **5**, 306 (1972).

¹⁷O. K. Andersen, H. L. Skriver, H. Nohl, and B. Johansson, Pure Appl. Chem. **52**, 93 (1979).

¹⁸J. Yamashita and S. Asano, J. Phys. Soc. Jpn. **52**, 3506 (1983).

¹⁹T. Oguchi, K. Terakura, and A. R. Williams, Phys. Rev. B **28**, 6443 (1983).

²⁰T. Oguchi, K. Terakura, and A. R. Williams, J. Appl. Phys. **55**, 2318 (1984).

²¹See Ref. 19, and references therein.

²²K. Terakura, A. R. Williams, T. Oguchi, and J. Kübler, Phys. Rev. Lett. **52**, 1830 (1984).

²³S. Hufner and G. K. Wertheim, Phys. Rev. B **7**, 5086 (1973).

²⁴K. Terakura and A. R. Williams (unpublished).

²⁵A. R. Williams, J. Kübler, and C. D. Gelatt, Jr., Phys. Rev. B **19**, 6094 (1979).

²⁶V. L. Moruzzi, J. F. Janak, and A. R. Williams, *Calculated Electronic Properties of Metals* (Pergamon, New York, 1978).

- ²⁷The band-energy contribution to the stabilization of AF II due to the intersublattice hybridization is cancelled to some extent by the change in the exchange energy $-(I/4)M_{\text{loc}}^2$ (I , intra-atomic exchange integral; M_{loc} , magnitude of local magnetic moment), because the stronger intersublattice hybridization generally reduces M_{loc} more. Detailed discussions of this aspect in the case of Heusler alloys were given in J. Kübler, A. R. Williams, and C. B. Sommers, *Phys. Rev. B* **28**, 1745 (1983).
- ²⁸M. T. Hutchings and E. J. Samuelsen, *Solid State Commun.* **9**, 1011 (1971).
- ²⁹W. L. Roth, *Phys. Rev.* **110**, 1333 (1958).
- ³⁰J. Kanamori, *Prog. Theor. Phys.* **17**, 177 (1957); **17**, 197 (1957).
- ³¹T. Moriya, *Prog. Theor. Phys.* **33**, 157 (1965).
- ³²K. Yosida, A. Okiji, and S. Chikazumi, *Prog. Theor. Phys.* **33**, 559 (1965).
- ³³P. B. Coqblin and A. Blandin, *Adv. Phys.* **17**, 281 (1968).
- ³⁴J. F. Janak, *Phys. Rev. B* **16**, 255 (1977).
- ³⁵O. Gunnarsson, *J. Phys. F* **6**, 587 (1976).
- ³⁶In most of the Mott-insulator theories, the value of $U - J$ is assumed to be about 10 eV. However, as discussed in the Introduction and in Sec. III, some experimental data suggest that $U - J$ must be only about 2 eV.
- ³⁷J. F. Janak and A. R. Williams, *Phys. Rev. B* **23**, 6301 (1981).
- ³⁸B. E. F. Fender, A. J. Jacobson, and F. A. Wedgwood, *J. Chem. Phys.* **48**, 990 (1968).
- ³⁹H. A. Alperin, *J. Phys. Soc. Jpn. Suppl. B* **17**, 12 (1962).
- ⁴⁰D. C. Khan and R. A. Erickson, *Phys. Rev. B* **1**, 2243 (1970).
- ⁴¹The atomic radius for each atom is determined by using the atomic volume V_i and the bulk modulus B_i obtained by the band-structure calculation for each elemental material. The volume difference is allotted according to $\Delta V_1/\Delta V_2 = (B_2/B_1)(V_1/V_2)$, so that the given lattice parameter is reproduced.
- ⁴²L. Pauling, *Nature of the Chemical Bond* (Cornell University Press, Ithaca, 1945).
- ⁴³V. Heine, *Phys. Rev.* **153**, 673 (1967).